Quantification of Non-refractory Aerosol Nitrate in Ambient Air by Thermal Dissociation Cavity Ring-Down Spectroscopy

Natasha M. Garner[1], *Laura C. Matchett*[1,a] *and Hans D. Osthoff*[1]*

[1] Department of Chemistry, University of Calgary, 2500 University Drive NW, Calgary, Alberta, T2N 1N4, Canada

hosthoff@ucalgary.ca

[a] now at: Department of Chemistry, University of Alberta, 11227 Saskatchewan Drive, Edmonton, Alberta, T6G 2G2, Canada

Phone: 403-220-8689

Research article for *Environmental Science & Technology*

June 21, 2021

ABSTRACT

A thermal dissociation cavity ring-down spectrometer (TD-CRDS) for real-time quantification of non-refractory aerosol nitrate in ambient air is described. The instrument uses four parallel detection channels and heated quartz inlets to convert particulate organic nitrate (pON) (at 350 °C) and ammonium nitrate (NH_4NO_3) aerosol (at 540 °C) to nitrogen dioxide (NO_2), whose mixing ratio is monitored via its absorption at 405 nm. Concentrations of aerosol nitrate are determined by difference relative to a parallel TD-CRDS channel in which aerosol are removed by in-line filtering. The method was validated by sampling gas streams containing laboratory-generated NH_4NO_3 aerosol in parallel to a scanning mobility particle sizer (SMPS). Scatter plots of TD-CRDS and SMPS data correlated ($r^2 > 0.9$) with slopes near unity, confirming quantitative TD-CRDS response to NH_4NO_3 aerosol. In contrast, no response was observed when sampling $(NH_4)_2SO_4$ aerosol. Instrument limits of detection (LOD; 2σ, 10 s) were 120 parts per trillion by volume (10^{-12}, pptv) for NO_2 and 148 pptv for ammonium nitrate. Partial and unsustained conversion of refractory sodium nitrate ($NaNO_3$) was observed at the inlet temperature used for complete dissociation of HNO_3 and NH_4NO_3, suggesting that this channel may not constitute a robust measurement of total odd nitrogen (NO_y) in environments where $NaNO_3$ particles may be present (e.g., the polluted marine boundary layer). A potential application of TD-CRDS is the calibration of particle counters, for which convenient methods are not currently available. Sample ambient air measurements of pON and total aerosol nitrate in Calgary are presented.

KEYWORDS

aerosol nitrate, thermal dissociation, cavity ring-down spectroscopy, nitric acid, ammonium nitrate, sodium nitrate

INTRODUCTION

Ambient air concentrations of fine particulate matter (PM) are of interest since increased exposure to this criteria air pollutant has been linked to cardiovascular and pulmonary disease and early mortality.[1, 2] In recent years, decreasing sulfur dioxide (SO_2) emissions in Europe and North America have led to an increase in aerosol nitrate levels,[3] with inorganic nitrate now often the major fraction of total aerosol mass. For example, particulate nitrate was recently found to account for 16-35% of submicron aerosol in China[4] and upwards of 80% in the San Joaquin Valley, California[5] and Salt Lake Valley, Utah in winter.[6] Aerosol nitrate consists of ammonium nitrate (NH_4NO_3), organic nitrates (pON),[7] and less volatile salts such as sodium and calcium nitrate ($NaNO_3$ and $Ca(NO_3)_2$). The latter results mainly from uptake of nitric acid (HNO_3) or dinitrogen pentoxide (N_2O_5) on sea salt aerosol[8] or mineral dust.[9, 10]

Particulate nitrates are most commonly quantified by impaction on filters which are analyzed offline,[11] but are prone to evaporative loss[12, 13] of NH_4NO_3 and bounce error.[14] Alternatively, particulate nitrates are extracted into liquids followed by either online analysis by ion chromatography[15-17] or offline analysis by, for example, mass spectrometry[18] or infrared spectroscopy.[19] Online analysis of NH_4NO_3 and pON is possible by aerosol mass spectrometry (AMS),[20-23] but is limited to submicron and non-refractory aerosol.

Thermal dissociation (TD) to nitrogen dioxide (NO_2) has emerged as a novel, fast-response total odd nitrogen (NO_y)[24] measurement technique and has been applied to the quantification of pON[25] and NH_4NO_3 aerosol.[26] Following conversion, NO_2 is quantified by laser-induced fluorescence (TD-LIF),[27] cavity ring-down (TD-CRDS)[28] or cavity phase-shift (TD-CAPS)[29] spectroscopy. Quantification of pON requires an inlet temperature of ~450 °C similar to gas-phase organic nitrates,[25] while dissociation of NH_4NO_3 aerosol to NO_2 requires temperatures of ~600 °C and proceeds by a stepwise mechanism:[27, 30]

$$NH_4NO_{3(p)} \rightarrow NH_{3(g)} + HNO_{3(g)} \quad \text{(R1)}$$

$$HNO_{3(g)} \rightarrow NO_{2(g)} + OH_{(g)} \quad \text{(R2)}$$

The TD of $NaNO_3$ is believed to proceed by two main reactions, with the first yielding sodium monoxide (NaO) and NO_2,[30] and the second yielding sodium nitrite ($NaNO_2$) and atomic oxygen, followed by further decomposition of $NaNO_2$.[30-33]

$$NaNO_{3(s)} \rightarrow NaO_{(s)} + NO_{2(g)} \quad \text{(R3)}$$

$$NaNO_{3(s)} \rightarrow NaNO_{2(s)} + O_{(g)} \quad \text{(R4)}$$

Theoretical calculations[30] and some experimental results[31] suggest that R3 is favored over R4, though other studies[32, 33] reported $NaNO_2$ as the major product. Complicating matters, the presence of impurities (e.g., HNO_3 or NH_4NO_3)[30] and silica[33] may lower activation energies for TD of $NaNO_3$. Relevant to this paper, it has been reported that pure $NaNO_3$ "particles would not be detected in TD inlets"[26, 34] as NO_2.Though a temperature range over which this statement applies was not specified, it would have included the temperature needed to fully dissociate NH_4NO_3 of ~600 °C to ~650 °C. Quantification of $NaNO_3$ aerosol is possible with total reactive nitrogen (N_r) instruments[35, 36] that utilize catalysts at high temperatures to convert all atmospheric nitrogen species (other than N_2 and N_2O) to NO.

A general advantage of CRDS is that it is an absolute concentration measurement presuming the absorption cross-section of the target molecule is known and does not need to rely on external calibration.[37] Hence, TD-CRDS detection of NH_4NO_3 may potentially be used for the calibration of particle counting instruments (e.g., scanning mobility particle sizers (SMPS)). Although particle sizers can easily be calibrated with surfactant free polystyrene latex spheres,[38] quantification of particle counters remains a challenge and is often only performed against "trusted" counters.

Our group has developed and applied blue diode laser TD-CRDS for quantification of gas-phase components of NO_y, including NO_2,[39] NO,[40] total peroxyacyl nitrates ($\Sigma[PAN] = \Sigma[RC(O)O_2NO_2]$),[39] total alkyl nitrates ($\Sigma[AN] = \Sigma[RONO_2]$),[28] and nitryl chloride ($ClNO_2$).[41] Here, we describe the extension of this technique to the quantification of $HNO_{3(g)}$ and aerosol nitrate. The instrument was equipped with quartz inlet heaters modified for operation up to 700 °C. Gas streams containing laboratory-generated NH_4NO_3 or

85 $NaNO_3$ aerosol were analyzed by TD-CRDS in parallel to a SMPS. Applications of the new method such
86 as calibration of aerosol particle counters and quantification of aerosol nitrate in ambient air are presented
87 and discussed.

88 EXPERIMENTAL

89 **TD-CRDS**. An earlier version of the instrument and the measurement of NO_2 by blue diode laser CRDS
90 (whose accuracy is ~4%)[39] have been described elsewhere;[40] here, the design of the inlet for conversion of
91 particulate nitrates to NO_2 is presented. The instrument features four parallel measurement channels (Figure
92 1), color-coded for easier referencing as green, orange, purple and ash. Two channels were converted to
93 measure aerosol nitrate (ash and orange). The inlets for these channels were constructed using ¼" (0.635
94 cm) outer diameter (o.d.) conductive silicone tubing (TSI) to minimize electrostatic loss of particles to
95 tubing walls. TD occurred in ~61 cm long, ¼" (0.635 cm) o.d., externally heated quartz tubes. The heaters
96 were constructed by wrapping Nichrome wire (Resistance = 14.5 Ω) around a ~30 cm long section of each
97 quartz tube, which was then coated in a ceramic adhesive (Cotronics Resbond™ 919) in which a K-type
98 thermocouple was embedded. Inline filter holders, constructed from perfluororalkoxy (PFA) Teflon (Cole
99 Palmer, RK-06103-13) containing 47 mm diameter, 1 μm pore size polytetrafluoroethylene (PTFE) filters
100 (Pall, R2PL047), were placed after each of the heated quartz tubes to prevent aerosol from entering the
101 optical cavities, similar to the instrument described by Wild et al.[24] To oxidize NO to NO_2, a gas stream
102 containing O_3 in O_2 was generated using a low-pressure Hg pen-ray lamp (Jelight, model 95-2100-2) and
103 a 10 μm critical orifice at 1.4×10^5 Pa O_2 cylinder gauge pressure and was added to the ash channel between
104 the converter and Teflon filter. The two remaining channels were as described previously[39] and sampled
105 from a shared Teflon filter holder assembly (Figure 1), quantifying NO_2 (green channel) and, depending on
106 convertor temperature, NO_2+ΣPAN or NO_2+ΣPAN+ΣAN or NO_2+ΣPAN+ΣAN+HNO_3 (purple channel).
107 The performance of these channels was evaluated using a diffusion source (see Supporting Information)
108 emitting trace amounts of NO_2, peroxyacetic and peroxypropanoic nitric anhydride (PAN and PPN),

isopropyl nitrate (IPN), and HNO_3. The instrument was operated at a flow rate of 2.4 standard Liters per minute (slpm) (0.6 slpm per channel) at near ambient pressure (~ 870 hPa).

Aerosol generation and size distribution measurements. Gas streams containing inorganic aerosol were generated using a commercial submicron aerosol generator (TSI). Aqueous solutions containing ~15 mM (Table S1) of NH_4NO_3 (Sigma-Aldrich), $NaNO_3$ (Sigma-Aldrich) or $(NH_4)_2SO_4$ (Fisher Scientific) were aspirated with nitrogen (Praxair) with an atomizer (model 3076). The generated mist was passed through a diffusion dryer (model 3062) containing silica beads to remove excess moisture and through an aerosol neutralizer (model 3012). Particles were size-selected using a differential mobility analyzer (DMA; model 3080) at a flow rate of 0.3 to 0.5 Liters per minute. The DMA output was combined with ultrapure air delivered from a cylinder (Praxair, "zero" grade) or from a zero-air generator via ¼" (0.635 cm) o.d. conductive silicone tubing (TSI) and stainless-steel fittings (Swagelok). Particle concentrations were varied by changing the output pressure of the N_2 gas cylinder.

The combined gas stream was analyzed in parallel by SMPS (TSI, DMA model 3080 and condensation particle counter model 3775 operated with butanol) and TD-CRDS, with the excess flowing past a relative humidity probe (VWR) into an exhaust vent. The manufacturer-stated accuracy of the aerosol size distribution data is ±20%.

Ambient air measurements. Ambient air was sampled on the University of Calgary campus at the "Weather Research Station" site (latitude 51.07929˚N, longitude -114.14182˚W) on August 23, 2018. More information can be found in the Supporting Information.

RESULTS

TD curves. Figure 2A shows a representative TD-CRDS inlet temperature scan when a mixture containing constant amounts of the trace gases NO_2, PAN, PPN, IPN, and HNO_3 was sampled. The mixing ratios plateau in a similar fashion as first described by Day et al.[27] The solid line is a multivariate fit of

equation E1, which is an extension of equation (4) of Paul et al.[28] to the data, using the software package Igor Pro (Wavemetrics Inc.).

$$[NO_2]_{total} = [NO_2]_0 + \Sigma[PAN]\times\left(1\text{-}e^{-A_{PAN}\times e^{\frac{-E_{A,PAN}}{RT}}\times t_{res}}\right) + \Sigma[AN]\times\left(1\text{-}e^{-A_{AN}\times e^{\frac{-E_{A,AN}}{RT}}\times t_{res}}\right)$$

$$+ [HNO_3]\times\left(1\text{-}e^{-A_{HNO_3}\times e^{\frac{-E_{,A,HNO_3}}{RT}}\times t_{res}}\right) \quad \text{(E1)}$$

Here, $[NO_2]_{total}$ is the NO_2 mixing ratio observed by CRDS, $[NO_2]_0$, Σ[PAN], Σ[AN], and $[HNO_3]$ are the mixing ratios of each NO_y component in the sampled air, R is the universal gas constant (8.314 J mol^{-1} K^{-1}), A and E_A are Arrhenius parameters for TD of PAN, IPN, and HNO_3, respectively (Table 1), and t_{res} is the time that the gas spends in the converter at the heater set temperature, T. Even though E1 neglects axial and radial temperature gradients, secondary chemistry in the quartz inlet, and assumes a temperature-independent t_{res} and is thus semiempirical, it allows for reasonable simulation of TD profiles.[41] Fits using a modified version of (E1) in which t_{res} was normalized by multiplication with a factor of (273.15/T) yielded equivalent results (data not shown).

A fit of E1 to the data in Figure 2A gave t_{res} = 34.4±0.4 ms, $[NO_2]$ = 0.727±0.004 ppbv, Σ[PAN] = 0.658±0.007 ppbv, Σ[AN] = 0.62±0.01 ppbv, and $[HNO_3]$ = 5.28±0.01 ppbv, where the errors are estimated standard deviations of the fit coefficients calculated by the closed-source algorithm within Igor Pro.

Upon close inspection, it is apparent that TD of HNO_3 commences prior to complete TD of IPN, a phenomenon recently noted by Womack et al.[26] For the data in Figure 2A the effect on quantification of Σ[AN] is small: At T = 358 °C, for example, 99.95% of IPN and 0.07% of HNO_3 are predicted (using E1) to dissociate. If the TD instrument were operated with its inlet maintained at a fixed temperature, a common mode of operation in other TD instruments,[26, 27, 42] the contribution of HNO_3 to the $[NO_2]+\Sigma[PAN]+\Sigma[AN]$ signal would be larger than predicted by E1 but likely still be negligible compared to the error introduced by the subtraction of NO_2 between channels. As noted by others,[26, 43] performance varies between inlet

heaters and operating temperature and pressure, which can lead to greater overlap of the TD curves of IPN and HNO_3, such that the contribution of HNO_3 to the $[NO_2]+\Sigma[PAN]+\Sigma[AN]$ signal would have be investigated in each inlet.

Figure 2B shows a TD-CRDS inlet temperature scan when a constant amount of HNO_3 was sampled at near-ambient pressure of ~870 hPa. A fit of E1 to this temperature scan (with $[NO_2]_0 = \Sigma[PAN] = \Sigma[AN]$ constrained to 0 ppbv) gave $[HNO_3]$ = 77.5±0.8 ppbv and a residence time t_{res} = 166±10 ms.

Superimposed is a TD scan (data points shown in red) when NH_4NO_3 aerosol was sampled under identical conditions. A fit of E2 to these data,

$$[NO_2]_{total} = [NO_{3(p)}] \times \left(1\text{-}e^{-A_{NO_{3(p)}} \times e^{\frac{-E_{A,NO_{3(p)}}}{RT}} \times t_{res}} \right) \quad \text{(E2)}$$

constrained to t_{res} = 166 ms and the pre-exponential factor of HNO_3, yielded a mixing ratio of 33.58±0.06 ppbv and an effective activation energy $E_A^*{}_{NH4NO3}$ = 203.68±0.07 kJ mol^{-1}. The value of $E_A^*{}_{NH4NO3}$ is consistent with the activation energy for NO_2 production from HNO_3 (R2), i.e., the mechanism proposed by Day et al. [27] and Cagnina et al.[30] The accuracy of E_A^* values derived by fitting E2 is lower than suggested by the fit error since E2 only approximates the TD profile.

The TD-CRDS response to NH_4NO_3 aerosol was not affected by addition of O_3 between the TD section and the CRDS cell (see "Interference tests" section), which indicated that NO is not a product of NH_4NO_3 thermal decomposition. A sigmoidal TD curve was also observed when $NaNO_3$ aerosol was sampled (Figure 2B; shown in cyan color). This curve plateaus at higher temperatures than required to dissociate other NO_y components (Figure S3). There was no response when $NaNO_2$ aerosol was analyzed (up to an inlet temperature of 640 °C), other than a gas-phase signal due to HONO(g) when O_3 was added (data not shown), suggesting that $NaNO_2$ aerosol is not an intermediate product in the TD of $NaNO_3$.

The TD of $NaNO_3$ occurs from ~450 °C to ~650 °C, at temperatures that are too low to be reconciled with the Arrhenius parameters reported by Bond and Jacobs.[32] A fit of E2 with the $E_{A,NaNO3}$ of 187 kJ mol^{-1} reported by Freeman[31] and t_{res} = 166 ms gives a pre-exponential factor $A^*_{NaNO3} = (6.05\pm0.08)\times10^{-12}$ s^{-1} and a mixing ratio of 19.88±0.06 ppbv. A fit of E2 constrained to the pre-exponential factor of HNO_3 gave $E_A{}^*_{NaNO3}$ = 225.7±0.1 kJ mol^{-1} and a mixing ratio of 19.87±0.07 ppbv (shown as a solid line in Figure 2B). The quality of these fits is somewhat poorer than those of IPN, HNO_3, or NH_4NO_3, with noticeable deviations at the upper temperature range of the curve. In particular, the fit shown in Fig. 2B predicts a plateau at temperatures >590 °C, yet the observed mixing ratios continue to rise by an additional 6% to 21.0±0.2 ppbv at temperatures >615 °C. It is unclear if this is due to occurrence of multiple stages[32] in the TD of $NaNO_3$ or due to uneven heating and temperature gradients of the gas stream, which would be more pronounced at the higher temperatures. The notion of multiple decomposition pathways with separate activation barriers is supported by a double-exponential fit (constrained to A_{HNO3}) which reproduces the data (not shown); this fit indicates that 15.0±0.1 ppbv of the $NaNO_3$ converted to NO_2 with $E_A{}^*_{NaNO3,1}$ = 222.2±0.9 kJ mol^{-1} and the remainder (5.8±0.1 ppbv) with $E_A{}^*_{NaNO3,2}$ = 241±3 kJ mol^{-1}.

Simultaneous quantification of NH_4NO_3 aerosol by TD-CRDS and SMPS. Figure 3 shows time series of SMPS and TD-CRDS data when both instruments sampled size-selected, laboratory-generated NH_4NO_3 aerosol in parallel. In this experiment, the aerosol flow was by-passed every 5 - 10 min for ~5 min to determine the "zero" ring-down time constant (τ_0) of the TD-CRDS; furthermore, the particle concentration was altered during the zeroing periods by changing the cylinder pressure of the aerosol generation system.

The size distribution data (Figure 3A) show that multiple particle modes were, in fact, delivered by the aerosol generation system. From these data, time series of aerosol volume and mass densities were calculated and converted to equivalent NO_2 mixing ratios, assuming spherical particle size and using particle density calculated using E-AIM[44] (Table S1).

$$\text{SMPS } NO_2 \text{ equivalent mixing ratio} = \frac{\text{Aerosol number density}}{\text{Air number density}} = \frac{V \times \rho / M}{\text{Air number density}} \quad \text{(E3)}$$

Here, V is the aerosol volume density (in nm^3 cm^{-3}), ρ is the particle density (in g cm^{-3}) and M is the molecular weight of the nitrate salt (in g mol^{-1}). The air number density was calculated using the ideal gas law. The corresponding time series of equivalent NO_2 mixing ratios is shown in Figure 3B (black circles). These mixing ratios have a systematic uncertainty of ±36% (±20% uncertainty in particle counting, ±30% particle volume determination); this uncertainty is depicted in Figure 3B as a gray shaded area. Potential particle losses in the transfer lines are not included in this error estimate, which is likely a lower limit.

Superimposed are the TD-CRDS aerosol (shown in blue) and gas-phase NO_y (shown in red) data. There was very little response in the gas-phase channel (<1% of the response in the aerosol channel), confirming efficient particle removal by the filter and high selectivity between the gas and aerosol channels. The TD-CRDS aerosol data are precise with a typical relative standard deviation (RSD) of ~0.5% (10 s data) and respond rapidly (within seconds) to changes in particle concentration delivered. When sampling zero air, the 2σ precision of the TD-CRDS channel was ±148 pptv, corresponding to an aerosol mass density of ±0.32 μg (NO_3^-) m^{-3}. For quantification of ammonium nitrate in ambient air, the measurement precision may be larger (i.e., degrade) when a large and variable background signal needs to be subtracted, or when the aerosol concentration varies.

The insert in Figure 3B shows a scatter plot of NO_2 mixing ratios calculated using the TD-CRDS aerosol channel against those calculated from the SMPS data (E3). This plot has a slope near unity (1.03 ± 0.04) and a large Pearson correlation coefficient (r^2 = 0.932). Scatter plots of data collected in subsequent experiments (not shown) were also linear with slopes scattered around unity (Table S2). On aggregate, the conversion of ammonium nitrate to NO_2 in the TD-CRDS inlet is quantitative, at least within our ability to deliver and quantify NH_4NO_3 aerosol by SMPS.

Simultaneous quantification of $NaNO_3$ aerosol by TD-CRDS and SMPS. Data from a sample experiment with $NaNO_3$ aerosol are shown in Figure 4. The performance of TD-CRDS with $NaNO_3$ parallels that for NH_4NO_3 aerosol: The data are precise (2σ precision of ±145 pptv, corresponding to an aerosol mass density of ±0.26 μg (NO_3^-) m^{-3}), respond rapidly to concentration changes, and are correlated with concentrations observed by the SMPS (r^2 = 0.965). The slope of TD-CRDS to SMPS data was 0.98±0.03 in this experiment and is consistent with quantitative conversion of $NaNO_3$ to NO_2. In some experiments (Table S3), when the experiments were conducted over periods exceeding several hours, the ratio of TD-CRDS to SMPS concentrations gradually decreased (e.g., Figure S4) for reasons that are unclear. The TD-CRDS response to $NaNO_3$ could be restored by sampling NH_4NO_3 intermittingly (Figure S4).

Interference tests. A few interference tests were conducted to verify the robustness of TD of NH_4NO_3. The TD-CRDS response was not affected by changing relative humidity, as expected (Figure S5). Upon addition of O_3 up to a parts-per-million (ppmv) mixing ratio between the TD section and the CRDS cell, no change in TD-CRDS signal was observed (Figure S6), verifying that NO was not generated during the TD of NH_4NO_3 or $NaNO_3$. This was further verified by the addition of $(NH_4)_2SO_4$ aerosol in the presence of O_3 (Figure S8) where no change in TD-CRDS signal occurred assuring NH_4^+ did not convert to NO or NO_2 during thermal dissociation. Furthermore, the 1:1 stoichiometric response to NH_4NO_3 and absence of a response to $(NH_4)_2SO_4$, both of which liberate NH_3 when heated, infers the absence of a TD-CRDS response to NH_3.

Sample ambient air measurements. Figure 5 shows a time series and inlet temperature scan from ambient measurements conducted on Aug 23rd, 2018 at the University of Calgary. During the measurement period, the area was blanketed in biomass burning smoke originating from forest fires in British Columbia and Washington State with $PM_{2.5}$ of 96 μg m^{-3} and elevated levels of NO_x and O_3 (Table S4 and Figure S2).

Mixing ratios for the aerosol channel (blue trace) and reference channel (red trace) are shown in Figure 5A. The difference between the channels, i.e., the contribution from aerosol nitrate, is shown in green. A maximum of 24.3 ppbv $NO_3^-_{(p)}$ + $NO_{y(g)}$ (blue trace), 23.7 ppbv of $NO_{y(g)}$ (red trace, with an average of 12±6 ppbv) and 1.7 ppbv $NO_3^-_{(p)}$ were observed. The median 2σ precision of the $NO_3^-_{(p)}$ data was ±150 pptv for 10 s data and ±200 pptv for 60 s data. TD-CRDS NO_y and NO_x data (Figure S2) exhibited a similar time series. Spikes in the TD-CRDS NO_y data resulted from periodic vehicle traffic on a nearby road and was confirmed by elevated NO_x mixing ratios (Figure S2).

A time series of total aerosol nitrate concentration (in μg (NO_3^-) m^{-3}) is shown in Figure 5B, which was calculated by converting the CRDS mixing ratio for aerosol nitrate (in ppbv) using a conversion factor of 2.3 μg (NO_3^-) m^{-3} $ppbv^{-1}$. During the sampling period $NO_3^-_{(p)}$ fluctuated between 1-4 μg m^{-3}, with an average concentration of ~2 μg (NO_3^-) m^{-3} (median 2σ precision ±0.35 and ±0.46 μg (NO_3^-) m^{-3} for 10 s and 60 s data, respectively). Assuming full transmission and conversion of particulate nitrate within our inlet, this would represent between 1-4% of total $PM_{2.5}$ measured during this period.

Figure 5C shows an ambient temperature scan of the aerosol channel. During the time of this scan, the NO_z (= NO_y - NO_x) mixing ratio was constant (gray shaded region of Figure S2). Significant NO_x was present during this period (Figure S2), and the majority of the signal observed <200 °C resulted from NO_2. Fitting temperature scan data using E1 gave mixing ratios for Σ[AN] + pON = 0.80±0.05 ppbv and HNO_3 + $NH_4NO_{3(p)}$ = 0.97±0.04 ppbv. In a preliminary experiment, we examined pON generated in a smog chamber from reaction of limonene with nitrate radical (NO_3) and observed full dissociation of all nitrates at temperatures <450 ºC, consistent with literature.[27] Thus, pON likely contributed to the observed aerosol signal since the site was heavily impacted by biomass burning aerosol which contain pON.[45]

DISCUSSION

A new TD-CRDS for quantification of aerosol nitrate in laboratory and field studies has been described. Conversion of NH_4NO_3 aerosol to NO_2 occurred at inlet temperatures of 600 ºC, which is consistent with TD of HNO_3 and dissociation through the stepwise mechanism proposed by Day et al.[21] and Cagnina et al.[30] This conversion appears to be quantitative, as judged from simultaneous aerosol measurements by SMPS with an uncertainty of ±36%. The ability to selectively quantify HNO_3 and total NH_4NO_3 aerosol in ambient air is valuable, e.g., to quantify rates of NO_x oxidation to HNO_3 during day and N_2O_5 to HNO_3 at night. This is particularly useful, since existing online sampling techniques such as AMS only measure submicron particles and do not provide a total aerosol nitrate concentration or require relatively long sampling times of ~ 1 hr such as the particle-into-liquid sampler (PILS),[15] the ambient ion monitor (AIM)[16] or Monitor for AeRosols and GAses in ambient air (MARGA).[17]

The TD-CRDS measurements of NH_4NO_3 were validated against concentrations derived from size distribution data. A potential application of TD-CRDS is the reverse, i.e., calibration of SMPS responses via TD-CRDS measurements. Calibration methods for particle counters are in short supply and needed since the common "calibration" method is comparison to "trusted" particle counters. Furthermore, this could be expanded to include calibration against any well quantified NO_y measurement, (e.g., NO_x analyzer), increasing the ability to verify particle counter response to more widely available instrumentation.

We demonstrated that it is possible to quantify mixtures containing NO_2+ΣPAN+ΣAN+HNO_3 by fitting TD scan data for a single TD channel. This constitutes an advancement since conventional TD instruments use dedicated channels to continuously monitor at fixed relative temperatures and do not accurately quantify ΣAN and HNO_3 due to partial overlap of their TD profiles. Although less convenient, fitting scan data allows for the simultaneous analysis of additional components without instrument modification.

This instrument adds to a growing list of TD instruments[24, 25, 27-29] for the measurement of gas-phase and particulate NO_y, and work presented here should be of interest to this growing community or anyone relying on TD data. We have identified that measurement of NO_y by TD-CRDS may not be quantitative in all

environments (e.g., places impacted by $NaNO_3$ aerosol) due to the partial conversion of $NaNO_3$ at inlet temperatures of <660 ºC. Contrary to earlier studies that examined $NaNO_3$ and determined that those particles would not be detected in TD inlets,[26] we found a significant albeit non-quantitative response to $NaNO_3$ (Figure S4). However, further determination is required as it appears that $NaNO_3$ may convert more readily to NO_2 in the presence of NH_4NO_3 (or when NH_4NO_3 is co-sampled), which may assist field measurements since ambient aerosol is far more complex than pure laboratory samples.

The use of inlet filters to suppress aerosol is in contrast to the denuder method described by Rollins et al.[25] in which gas-phase species are suppressed. The latter has been used to measure pON and offers a higher signal-to-noise ratio since, unlike the filter method, does not require subtraction of two large signals (total minus gas-phase only channel). On the other hand, it is unclear if NH_4NO_3 would be efficiently transmitted through a denuder designed for complete removal of gas-phase species due to NH_4NO_3 particle evaporation and subsequent loss of HNO_3 and NH_3 to the denuder walls.

Future work. Future studies should investigate use of denuders for quantification of NH_4NO_3 in TD instruments and the TD of $NaNO_3$, in particular its mechanism. The preliminary smog chamber experiment with pON showed multiple (i.e., two) inflection points in the TD curves (data not shown), which are also vaguely visible in Figure 5C. There is a need for pON standards (currently lacking) to identify the types of organic nitrates involved. For future experiments, we intend to replace the silicone with conductive PFA Teflon tubing to avoid potential measurement artifacts.[46, 47]

Supporting information:

Description of synthesis and delivery of gases; schedule of experiments; description of ambient air measurements and setup including table summarizing auxiliary data and time series of TD-CRDS NO_x, NO_y and NO_z data; summary plot of normalized TD curves; additional TD-CRDS analysis of $NaNO_3$, $(NH_4)_2SO_4$ and NH_4NO_3; test for NO production; relative humidity test; O_3 interference test; other SI figures and tables mentioned herein.

Notes:

The authors declare no competing financial interest.

ACKNOWLEDGMENTS

This work was supported in part by Natural Sciences and Engineering Research Council of Canada (NSERC) in the form of a Discovery grant. N.M.G. acknowledges funding from a Queen Elizabeth II Graduate Scholarship. The authors thank Dr. Arthur Chan at the University of Toronto and Dr. Jose Jimenez at the University of Colorado for helpful discussions.

326 TABLES

327 **Table 1**: Parameters for thermal dissociation.

Compound	A (10^{15} s^{-1})	E_a (kJ mol^{-1})	E_a* (kJ mol^{-1})	Reference
$CH_3C(O)O_2NO_2$ (PAN)	25	113	-	[48]
i-$C_3H_7ONO_2$ (IPN)	3.98	136	-	[49]
HNO_3	2.0	205		[50]
NH_4NO_3	2.0**	-	204	this work
$NaNO_3$	2.0**	-	226 (222, 241)	this work

328 * derived from fits to the observed profiles; ** constrained.

329

330 FIGURES

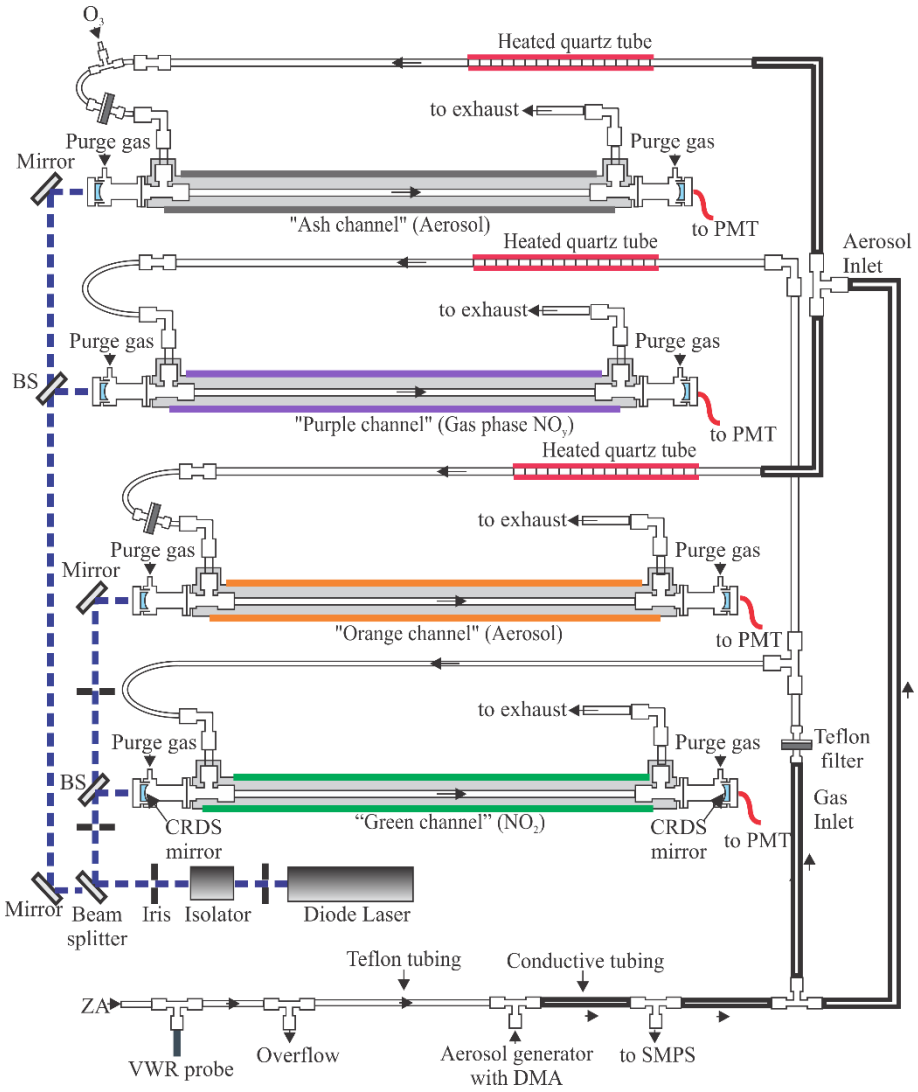

331

332 **Figure 1**. Schematic (not to scale) of the thermal dissociation cavity ring-down spectrometer (TD-CRDS).
333 The instrument features two channels for the quantification of NO_y including aerosol nitrate (ash and
334 orange) and two channels for quantification of NO_2 (green) and gas-phase NO_y (purple), i.e., NO_2+
335 Σ[PAN]+Σ[AN]+HNO_3. BS = beam splitter, ZA = zero air, DMA = differential mobility analyzer, SMPS
336 = scanning mobility particle sizer, PMT = photomultiplier tube.

337

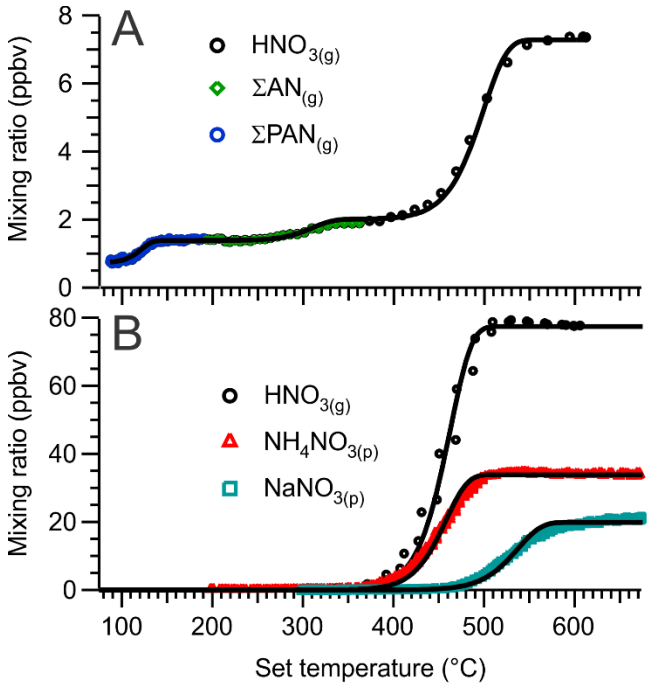

338

339 **Figure 2**. (A) TD-CRDS response as a function of inlet set temperature when sampling a mixture of
340 0.727±0.004 ppbv NO_2, 0.658±0.007 ppbv ΣPAN (blue circles ○; mixture of PAN and PPN), 0.624±0.012
341 ppbv ΣAN (green diamonds ◊; isopropyl nitrate), and 5.279±0.012 ppbv HNO_3 (black circles ○). In this
342 example, the TD-CRDS was operated at a sample cell pressure of 632 hPa, achieved by inserting a flow
343 restriction prior to the TD quartz cell. The solid line is a fit of E1 to the data, from which the mixing ratios
344 were obtained. (B) TD-CRDS response as a function of inlet set temperature when sampling 77.5±0.8 ppbv
345 of HNO_3 (black circles ○), 33.85±0.06 ppbv equivalent of NH_4NO_3(p) (red triangles Δ), and 19.87±0.07
346 ppbv equivalent of $NaNO_3$(p) (cyan squares, □). The solid black lines are fits of equations E1 (HNO_3) and
347 E2 ($NO_{3(p)}$) to the data.

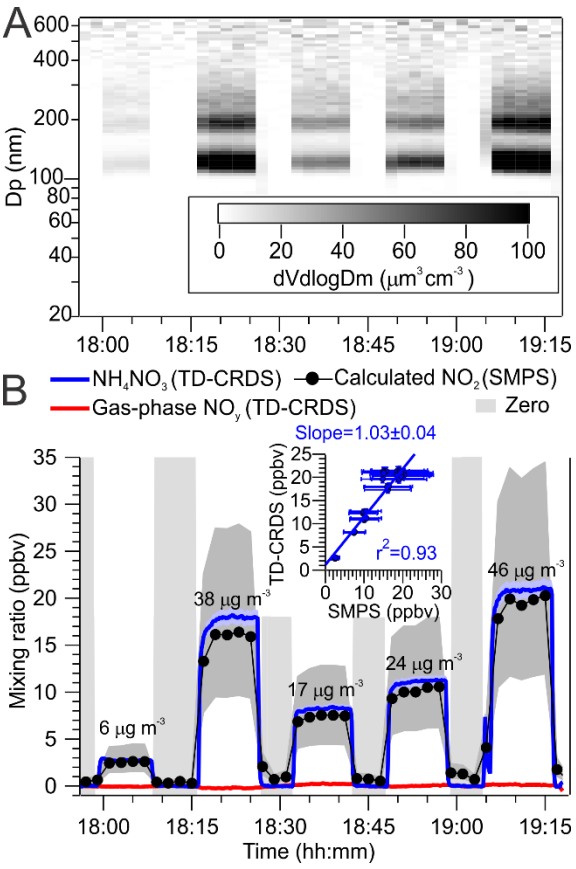

348

349 **Figure 3**. Analysis of size-selected (~150 nm) NH_4NO_3 aerosol by TD-CRDS and SMPS. (**A**) Time series
350 of aerosol size distribution data. (**B**) Corresponding time series of NO_2 equivalent mixing ratios (black
351 circles) and TD-CRDS gas-phase NO_y and aerosol nitrate measured at inlet temperatures of 600 °C (red
352 and blue traces). The area shown in dark gray indicates the SMPS measurement uncertainty. The light-gray
353 underlay indicates periods when both instruments sampled aerosol-free air. The insert is a scatter plot of
354 the TD-CRDS and SMPS derived mixing ratios (see text).

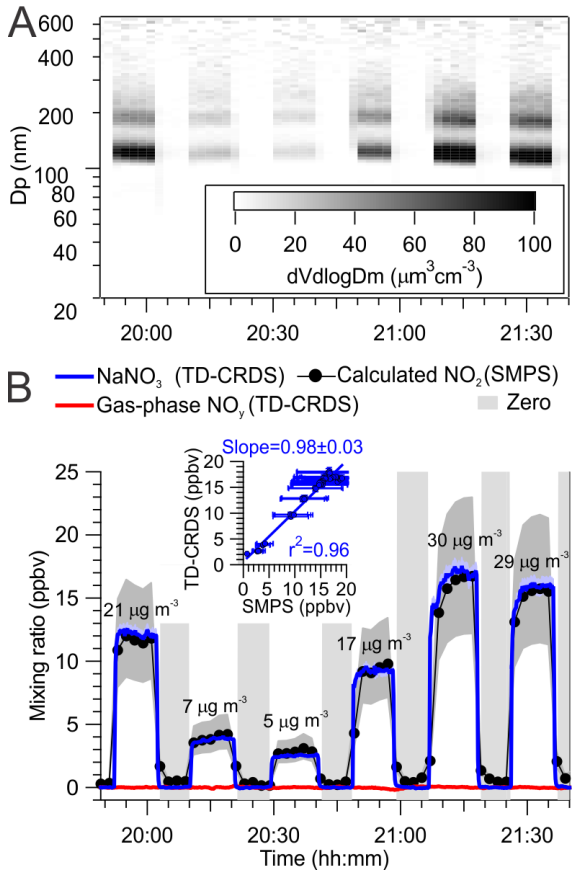

355

356 **Figure 4**. Analysis of size-selected (~150 nm) $NaNO_3$ aerosol by TD-CRDS and SMPS. (**A**) Time series
357 of aerosol size distribution data. (**B**) Corresponding time series of NO_2 equivalent mixing ratios (black
358 circles) and TD-CRDS gas-phase NO_y and aerosol nitrate measured at inlet temperature of 600-620 °C (red
359 and blue traces). The insert is a scatter plot of the TD-CRDS and SMPS data.

360

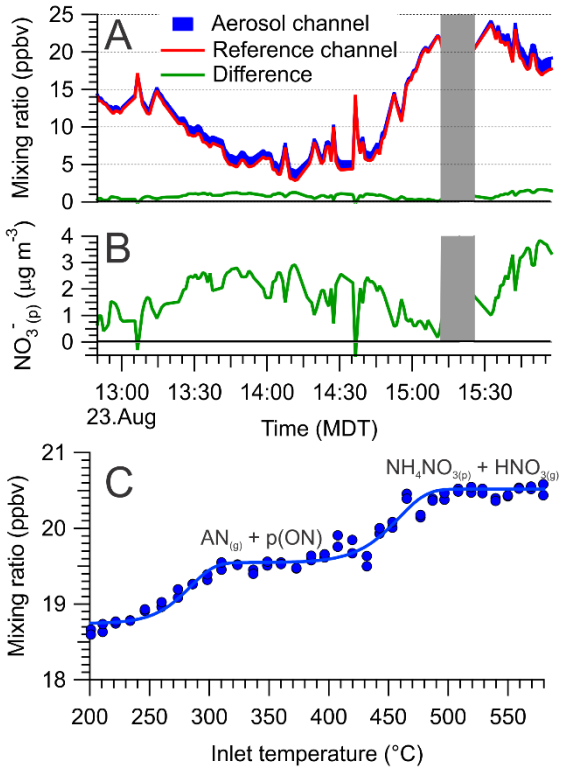

361

362 **Figure 5**. (**A**) Time series of ambient air TD-CRDS mixing ratios (averaged to 1 min) observed in Calgary
363 on Aug 23, 2018. (**B**) Time series of total aerosol nitrate concentration, in µg (NO_3^-) m^{-3}. (**C**) Aerosol
364 channel temperature scan conducted between 15:22:25 to 15:24:13 Mountain Daylight Time (MDT). The
365 gray bars in panels (A) and (B) indicate this period and also include a 10 min period for the inlet to cool
366 prior to the temperature scan.

367

368 REFERENCES

369 1. Pope, C. A.; Ezzati, M.; Dockery, D. W., Fine-Particulate Air Pollution and Life
370 Expectancy in the United States. *N. Engl. J. Med.* **2009,** *360*, (4), 376-386.

371 2. Lelieveld, J.; Evans, J. S.; Fnais, M.; Giannadaki, D.; Pozzer, A., The contribution of
372 outdoor air pollution sources to premature mortality on a global scale. *Nature* **2015,** *525*, (7569),
373 367-371.

374 3. Hand, J. L.; Gebhart, K. A.; Schichtel, B. A.; Malm, W. C., Increasing trends in wintertime
375 particulate sulfate and nitrate ion concentrations in the Great Plains of the United States (2000–
376 2010). *Atmos. Environm.* **2012,** *55*, (0), 107-110.

377 4. Li, Y. J.; Sun, Y.; Zhang, Q.; Li, X.; Li, M.; Zhou, Z.; Chan, C. K., Real-time chemical
378 characterization of atmospheric particulate matter in China: A review. *Atmos. Environm.* **2017,**
379 *158*, 270-304.

380 5. Parworth, C. L.; Young, D. E.; Kim, H.; Zhang, X.; Cappa, C. D.; Collier, S.; Zhang, Q.,
381 Wintertime water-soluble aerosol composition and particle water content in Fresno, California. *J.*
382 *Geophys. Res.-Atmos.* **2017,** *122*, (5), 3155-3170.

383 6. Baasandorj, M.; Hoch, S. W.; Bares, R.; Lin, J. C.; Brown, S. S.; Millet, D. B.; Martin, R.;
384 Kelly, K.; Zarzana, K. J.; Whiteman, C. D.; Dube, W. P.; Tonnesen, G.; Jaramillo, I. C.; Sohl, J.,
385 Coupling between Chemical and Meteorological Processes under Persistent Cold-Air Pool
386 Conditions: Evolution of Wintertime $PM_{2.5}$ Pollution Events and N_2O_5 Observations in Utah's Salt
387 Lake Valley. *Environm. Sci. Technol.* **2017,** *51*, (11), 5941-5950.

388 7. Lee, B. H.; Mohr, C.; Lopez-Hilfiker, F. D.; Lutz, A.; Hallquist, M.; Lee, L.; Romer, P.;
389 Cohen, R. C.; Iyer, S.; Kurten, T.; Hu, W. W.; Day, D. A.; Campuzano-Jost, P.; Jimenez, J. L.;
390 Xu, L.; Ng, N. L.; Guo, H. Y.; Weber, R. J.; Wild, R. J.; Brown, S. S.; Koss, A.; de Gouw, J.;

391 Olson, K.; Goldstein, A. H.; Seco, R.; Kim, S.; McAvey, K.; Shepson, P. B.; Starn, T.; Baumann,
392 K.; Edgerton, E. S.; Liu, J. M.; Shilling, J. E.; Miller, D. O.; Brune, W.; Schobesberger, S.;
393 D'Ambro, E. L.; Thornton, J. A., Highly functionalized organic nitrates in the southeast United
394 States: Contribution to secondary organic aerosol and reactive nitrogen budgets. *Proc. Natl. Acad.*
395 *Sci. U.S.A.* **2016,** *113*, (6), 1516-1521.
396 8. Fitzgerald, J. W., Marine Aerosols - A Review. *Atmos. Environm. A* **1991,** *25*, (3-4), 533-
397 545.
398 9. Allen, H. M.; Draper, D. C.; Ayres, B. R.; Ault, A.; Bondy, A.; Takahama, S.; Modini, R.
399 L.; Baumann, K.; Edgerton, E.; Knote, C.; Laskin, A.; Wang, B.; Fry, J. L., Influence of crustal
400 dust and sea spray supermicron particle concentrations and acidity on inorganic NO_3^- aerosol
401 during the 2013 Southern Oxidant and Aerosol Study. *Atmos. Chem. Phys.* **2015,** *15*, (18), 10669-
402 10685.
403 10. Pan, X. L.; Uno, I.; Wang, Z.; Nishizawa, T.; Sugimoto, N.; Yamamoto, S.; Kobayashi, H.;
404 Sun, Y. L.; Fu, P. Q.; Tang, X.; Wang, Z. F., Real-time observational evidence of changing Asian
405 dust morphology with the mixing of heavy anthropogenic pollution. *Scientific Reports* **2017,** *7*.
406 11. Zhuang, H.; Chan, C. K.; Fang, M.; Wexler, A. S., Size distributions of particulate sulfate,
407 nitrate, and ammonium at a coastal site in Hong Kong. *Atmos. Environm.* **1999,** *33*, (6), 843-853.
408 12. Zhang, X. Q.; McMurry, P. H., Theoretical analysis of evaporative losses of adsorbed or
409 absorbed species during atmospheric aerosol sampling. *Environm. Sci. Technol.* **1991,** *25*, (3), 456-
410 459.
411 13. Hering, S.; Cass, G., The magnitude of bias in the measurement of $PM_{2.5}$ arising from
412 volatilization of particulate nitrate from teflon filters. *J. Air Waste Manag. Assoc.* **1999,** *49*, (6),
413 725-733.

14. Dzubay, T. G.; Hines, L. E.; Stevens, R. K., Particle bounce errors in cascade impactors. *Atmos.Environm. (1967)* **1976,** *10*, (3), 229-234.

15. Weber, R. J.; Orsini, D.; Daun, Y.; Lee, Y. N.; Klotz, P. J.; Brechtel, F., A particle-into-liquid collector for rapid measurement of aerosol bulk chemical composition. *Aerosol Sci. Technol.* **2001,** *35*, (3), 718-727.

16. Markovic, M. Z.; VandenBoer, T. C.; Murphy, J. G., Characterization and optimization of an online system for the simultaneous measurement of atmospheric water-soluble constituents in the gas and particle phases. *J. Environ. Monit.* **2012,** *14*, (7), 1872-1884.

17. Rumsey, I. C.; Cowen, K. A.; Walker, J. T.; Kelly, T. J.; Hanft, E. A.; Mishoe, K.; Rogers, C.; Proost, R.; Beachley, G. M.; Lear, G.; Frelink, T.; Otjes, R. P., An assessment of the performance of the Monitor for AeRosols and GAses in ambient air (MARGA): a semi-continuous method for soluble compounds. *Atmos. Chem. Phys.* **2014,** *14*, (11), 5639-5658.

18. Li, R.; Wang, X. F.; Gu, R. R.; Lu, C. Y.; Zhu, F. P.; Xue, L. K.; Xie, H. J.; Du, L.; Chen, J. M.; Wang, W. X., Identification and semi-quantification of biogenic organic nitrates in ambient particulate matters by UHPLC/ESI-MS. *Atmos. Environm.* **2018,** *176*, 140-147.

19. Nielsen, T.; Egelov, A. H.; Granby, K.; Skov, H., Observations of particulate organic nitrates and unidentified components of NO_y. *Atmos. Environm.* **1995,** *29*, (15), 1757-1769.

20. Jayne, J. T.; Leard, D. C.; Zhang, X. F.; Davidovits, P.; Smith, K. A.; Kolb, C. E.; Worsnop, D. R., Development of an aerosol mass spectrometer for size and composition analysis of submicron particles. *Aerosol Sci. Technol.* **2000,** *33*, (1-2), 49-70.

21. Jimenez, J. L.; Jayne, J. T.; Shi, Q.; Kolb, C. E.; Worsnop, D. R.; Yourshaw, I.; Seinfeld, J. H.; Flagan, R. C.; Zhang, X. F.; Smith, K. A.; Morris, J. W.; Davidovits, P., Ambient aerosol sampling using the Aerodyne Aerosol Mass Spectrometer. *J. Geophys. Res.* **2003,** *108*, (D7), 8425.

22. Farmer, D. K.; Matsunaga, A.; Docherty, K. S.; Surratt, J. D.; Seinfeld, J. H.; Ziemann, P. J.; Jimenez, J. L., Response of an aerosol mass spectrometer to organonitrates and organosulfates and implications for atmospheric chemistry. *Proc. Natl. Acad. Sci. U.S.A.* **2010,** *107*, (15), 6670-6675.

23. Pratt, K. A.; Mielke, L. H.; Shepson, P. B.; Bryan, A. M.; Steiner, A. L.; Ortega, J.; Daly, R.; Helmig, D.; Vogel, C. S.; Griffith, S.; Dusanter, S.; Stevens, P. S.; Alaghmand, M., Contributions of individual reactive biogenic volatile organic compounds to organic nitrates above a mixed forest. *Atmos. Chem. Phys.* **2012,** *12*, (21), 10125-10143.

24. Wild, R. J.; Edwards, P. M.; Dube, W. P.; Baumann, K.; Edgerton, E. S.; Quinn, P. K.; Roberts, J. M.; Rollins, A. W.; Veres, P. R.; Warneke, C.; Williams, E. J.; Yuan, B.; Brown, S. S., A Measurement of Total Reactive Nitrogen, NO_y, together with NO_2, NO, and O_3 via Cavity Ring-down Spectroscopy. *Environm. Sci. Technol.* **2014,** *48*, (16), 9609-9615.

25. Rollins, A. W.; Smith, J. D.; Wilson, K. R.; Cohen, R. C., Real Time In Situ Detection of Organic Nitrates in Atmospheric Aerosols. *Environm. Sci. Technol.* **2010,** *44*, (14), 5540-5545.

26. Womack, C. C.; Neuman, J. A.; Veres, P. R.; Eilerman, S. J.; Brock, C. A.; Decker, Z. C. J.; Zarzana, K. J.; Dube, W. P.; Wild, R. J.; Wooldridge, P. J.; Cohen, R. C.; Brown, S. S., Evaluation of the accuracy of thermal dissociation CRDS and LIF techniques for atmospheric measurement of reactive nitrogen species. *Atmos. Meas. Tech.* **2017,** *10*, (5), 1911-1926.

27. Day, D. A.; Wooldridge, P. J.; Dillon, M. B.; Thornton, J. A.; Cohen, R. C., A thermal dissociation laser-induced fluorescence instrument for in situ detection of NO_2, peroxy nitrates, alkyl nitrates, and HNO_3. *J. Geophys. Res.* **2002,** *107*, (D5-6), D6, 4046.

28. Paul, D.; Furgeson, A.; Osthoff, H. D., Measurements of total peroxy and alkyl nitrate abundances in laboratory-generated gas samples by thermal dissociation cavity ring-down spectroscopy. *Rev. Sci. Instrum.* **2009,** *80*, (11), 114101.

29. Sadanaga, Y.; Takaji, R.; Ishiyama, A.; Nakajima, K.; Matsuki, A.; Bandow, H., Thermal dissociation cavity attenuated phase shift spectroscopy for continuous measurement of total peroxy and organic nitrates in the clean atmosphere. *Rev. Sci. Instrum.* **2016,** *87*, (7), 074102.

30. Cagnina, S.; Rotureau, P.; Singh, S.; Turcotte, R.; Fayet, G.; Adamo, C., Theoretical and Experimental Study of the Reaction between Ammonium Nitrate and Sodium Salts. *Ind. Eng. Chem. Res.* **2016,** *55*, (47), 12183-12190.

31. Freeman, E. S., The Kinetics of the Thermal Decomposition of Sodium Nitrate and of the Reaction between Sodium Nitrite and Oxygen. *J. Phys. Chem.* **1956,** *60*, (11), 1487-1493.

32. Bond, B. D.; Jacobs, P. W. M., The thermal decomposition of sodium nitrate. *J. Chem. Soc. A* **1966**, (9), 1265-1268.

33. Hoshino, Y.; Utsunomiya, T.; Abe, O., The Thermal Decomposition of Sodium Nitrate and the Effects of Several Oxides on the Decomposition. *Bull. Chem. Soc. Jpn* **1981,** *54*, (5), 1385-1391.

34. Bertram, T. H.; Cohen, R. C., A prototype instrument for the real time detection of semi-volatile organic and inorganic nitrate aerosol. *EOS Transactions, American Geophysical Union, Fall Meeting* **2003**, Abstract A51F-0740.

35. Marx, O.; Brummer, C.; Ammann, C.; Wolff, V.; Freibauer, A., TRANC - a novel fast-response converter to measure total reactive atmospheric nitrogen. *Atmos. Meas. Tech.* **2012,** *5*, (5), 1045-1057.

36. Stockwell, C. E.; Kupc, A.; Witkowski, B.; Talukdar, R. K.; Liu, Y.; Selimovic, V.; Zarzana, K. J.; Sekimoto, K.; Warneke, C.; Washenfelder, R. A.; Yokelson, R. J.; Middlebrook, A. M.; Roberts, J. M., Characterization of a catalyst-based conversion technique to measure total particulate nitrogen and organic carbon and comparison to a particle mass measurement instrument. *Atmos. Meas. Tech.* **2018,** *11*, (5), 2749-2768.

37. Brown, S. S., Absorption spectroscopy in high-finesse cavities for atmospheric studies. *Chem. Rev.* **2003,** *103*, (12), 5219-5238.

38. Kidd, C.; Perraud, V.; Finlayson-Pitts, B. J., Surfactant-free latex spheres for size calibration of mobility particle sizers in atmospheric aerosol applications. *Atmos. Environm.* **2014,** *82*, (0), 56-59.

39. Paul, D.; Osthoff, H. D., Absolute Measurements of Total Peroxy Nitrate Mixing Ratios by Thermal Dissociation Blue Diode Laser Cavity Ring-Down Spectroscopy. *Anal. Chem.* **2010,** *82*, (15), 6695-6703.

40. Odame-Ankrah, C. A. Improved detection instrument for nitrogen oxide species. University of Calgary, http://hdl.handle.net/11023/2006, 10.5072/PRISM/26475, Calgary, 2015.

41. Thaler, R. D.; Mielke, L. H.; Osthoff, H. D., Quantification of Nitryl Chloride at Part Per Trillion Mixing Ratios by Thermal Dissociation Cavity Ring-Down Spectroscopy. *Anal. Chem.* **2011,** *83*, (7), 2761-2766.

42. Sobanski, N.; Schuladen, J.; Schuster, G.; Lelieveld, J.; Crowley, J. N., A five-channel cavity ring-down spectrometer for the detection of NO_2, NO_3, N_2O_5, total peroxy nitrates and total alkyl nitrates. *Atmos. Meas. Tech.* **2016,** *9*, (10), 5103-5118.

43. Thieser, J.; Schuster, G.; Schuladen, J.; Phillips, G. J.; Reiffs, A.; Parchatka, U.; Pöhler, D.; Lelieveld, J.; Crowley, J. N., A two-channel thermal dissociation cavity ring-down

503 spectrometer for the detection of ambient NO_2, RO_2NO_2 and $RONO_2$. *Atmos. Meas. Tech.* **2016,**
504 *9*, (2), 553-576.
505 44. Clegg, S. L.; Brimblecombe, P.; Wexler, A. S., Thermodynamic model of the system H^+-
506 NH_4^+-SO_4^{2-}-NO_3^--H_2O at tropospheric temperatures. *J. Phys. Chem. A* **1998,** *102*, (12), 2137-2154.
507 45. Yan, C.; Tham, Y. J.; Zha, Q.; Wang, X.; Xue, L.; Dai, J.; Wang, Z.; Wang, T., Fast
508 heterogeneous loss of N_2O_5 leads to significant nighttime NO_x removal and nitrate aerosol
509 formation at a coastal background environment of southern China. *Sci. Tot. Environm.* **2019,** *677*,
510 637-647.
511 46. Yu, Y.; Alexander, M. L.; Perraud, V.; Bruns, E. A.; Johnson, S. N.; Ezell, M. J.; Finlayson-
512 Pitts, B. J., Contamination from electrically conductive silicone tubing during aerosol chemical
513 analysis. *Atmos. Environm.* **2009,** *43*, (17), 2836-2839.
514 47. Timko, M. T.; Yu, Z. H.; Kroll, J. H.; Jayne, J. T.; Worsnop, D. R.; Miake-Lye, R. C.;
515 Onasch, T. B.; Liscinsky, D.; Kirchstetter, T. W.; Destaillats, H.; Holder, A. L.; Smith, J. D.;
516 Wilson, K. R., Sampling Artifacts from Conductive Silicone Tubing. *Aerosol Sci. Technol.* **2009,**
517 *43*, (9), 855-865.
518 48. Bridier, I.; Caralp, F.; Loirat, H.; Lesclaux, R.; Veyret, B.; Becker, K. H.; Reimer, A.;
519 Zabel, F., Kinetic and Theoretical Studies of the reactions $CH_3C(O)O_2$+NO_2+M <->
520 $CH_3C(O)O_2NO_2$+M between 248 K and 393 K and between 30 Torr and 760 Torr. *J. Phys. Chem.*
521 **1991,** *95*, (9), 3594-3600.
522 49. Zaslonko, I. S.; Smirnov, V. N.; Tereza, A. M., High-temperature decomposition of methyl,
523 ethyl, and isopropyl nitrates in shock-waves. *Kinet. Catal.* **1993,** *34*, (4), 531-538.
524 50. Glänzer, K.; Troe, J., Thermal Decomposition of Nitrocompounds in Shock Waves. IV:
525 Decomposition of Nitric Acid. *Ber. Bunsenges. Phys. Chem.* **1974,** *78*, (1), 71-76.

526

527